NFLUX Satellite-Based Surface Radiative Heat Fluxes. Part II: Gridded Products

JACKIE C. MAY, CLARK ROWLEY, AND CHARLIE N. BARRON

Naval Research Laboratory, Stennis Space Center, Mississippi

ABSTRACT

The Naval Research Laboratory (NRL) ocean surface flux (NFLUX) system provides near-real-time satellite-based gridded surface heat flux fields over the global ocean within hours of the observed satellite measurements. NFLUX can serve as an alternative to current numerical weather prediction models—in particular, the U. S. Navy Global Environmental Model (NAVGEM)—that provide surface forcing fields to operational ocean models. This study discusses the satellite-based shortwave and longwave global gridded analysis fields, which complete the full suite of NFLUX-provided ocean surface heat fluxes. A companion paper discusses the production of satellite swath-level surface shortwave radiation and longwave radiation estimates. The swath-level shortwave radiation estimates are converted into clearness-index values. Clearness index reduces the dependency on solar zenith angle, which allows for the assimilation of observations over a given time window. An automated quality-control process is applied to the swath-level estimates of clearness index and surface longwave radiation. Then 2D variational analyses of the quality-controlled satellite esti- mates with background atmospheric model fields form global gridded radiative heat flux fields. The clearness- index analysis fields are converted into shortwave analysis fields to be used in other applications. Three-hourly shortwave and longwave analysis fields are created from 1 May 2013 through 30 April 2014. These fields are validated against observations from research vessels and moored-buoy platforms and compared with NAVGEM. With the exception of the mean bias, the NFLUX fields have smaller errors when compared with those of NAVGEM.

1. Introduction

The combination of latent and sensible turbulent heat fluxes and solar and longwave radiative heat fluxes largely determines the ocean surface heat budget. The heating and cooling of the ocean surface affect oceanic properties such as mixed-layer and sonic-layer depths, as well as atmospheric features such as stability and convection. Ocean forecast modeling is highly de- pendent on these ocean surface heat fluxes. Most often, the heat flux fields used to force ocean model forecasts— in particular, those of operational forecast models— are obtained from numerical weather prediction (NWP) products (Wallcraft et al. 2008), because they are able to provide timely global gridded products. NWP products can have large errors in atmospheric fields, do not give a closed global heat budget, and often have large regional biases (Curry et al. 2004; Wallcraft et al. 2008). In addition, ocean models require ocean- only atmospheric forcing fields; using NWP products

can introduce land contamination to the atmospheric variables (Kara et al. 2007).

An alternative to NWP products is satellite-based products. Satellite-based products are more likely to have similar characteristics over time and are also available at high temporal resolution (Smith et al. 2011). These products can have large uncertainties because of inaccuracies in additional input data and in the surface flux retrieval algorithms or methods (May et al. 2017). Satellite-based surface heat flux datasets over the global ocean have been produced and have been available for many years, and several studies have compared these products (Garratt et al. 1998; Smith et al. 2011; Wang et al. 2013). The focus of most of these prior studies and datasets is on the surface state parameters and turbulent heat fluxes rather than on the surface radiative heat fluxes. The study presented here focuses on the satellite- based gridded radiative heat flux estimates.

Several satellite-based gridded radiative heat flux products currently exist. The most recent versions of existing satellite-based global radiative datasets in- clude the International Satellite Cloud Climatology Project (ISCCP) D series (Rossow and Schiffer 1999;

Zhang et al. 2004); the Clouds and the Earth's Radiant Energy System (CERES) synoptic $1° \times 1°$ product (SYN1deg), edition 3a (Rutan et al. 2015); and the National Aeronautics and Space Administration (NASA) Global Energy and Water Exchanges project (formerly Global Energy and Water Cycle Experiment) (GEWEX) surface radiation budget (SRB), release 3.0 (Zhang et al. 2013, 2015). Each of these datasets contains 3-hourly high-quality global flux estimates used for climate research. The ISCCP and GEWEX SRB products are available for July 1983–December 2007. The CERES SYN1deg products are produced with a data latency of about 6 months after the actual satellite observations are taken. CERES SYN1deg data are currently available for July 2002–June 2016.

The Fast Longwave and Shortwave Radiative Flux (FLASHFlux) dataset was developed more recently as a rapid-release version of CERES SYN1deg to provide flux estimates within 1 week of the observed satellite measurements (Kratz et al. 2014). The FLASHFlux dataset is produced using modified versions of the algorithms and processing techniques developed for CERES SYN1deg. When the CERES SYN1deg product becomes available, it replaces the FLASHFlux product, and therefore there is not a long archive of FLASHFlux data available. The FLASHFlux dataset is useful for many near-real-time data needs, but the 1-week data latency is still too long to be used in operational real-time forecast models.

Because of the data latency of the current satellite-based products and the shortcomings of current NWP products, the Naval Research Laboratory (NRL) ocean surface flux system (NFLUX) was developed. NFLUX provides gridded satellite-based surface heat flux estimates over the global ocean within hours of the observed satellite measurements. The NFLUX system largely uses satellite measurements from polar-orbiting passive microwave sensors. As stated in May et al. (2016), which focuses on the gridded satellite-based state parameters and turbulent heat fluxes within the NFLUX system, the NFLUX fields can serve two primary purposes. First, these fields can be an alternative or correction to current NWP products used to provide the surface forcing to operational ocean models. Second, these fields provide a means for using satellite observations of the air–sea interface to assess and monitor NWP products and coupled models.

A discussion of how the satellite-based gridded surface radiative fluxes are produced is given in section 2. Section 3 describes the current NWP model being used as the primary source of forcing for U.S. Navy global ocean models: the Navy Global Environmental Model (NAVGEM; Hogan et al. 2014). The NFLUX fields are

validated against in situ data and compared with NAVGEM and CERES SYN1deg fields in section 4.

2. Global gridded surface radiative heat flux fields

The NFLUX system processes and assimilates satellite observations to produce ocean surface heat flux estimates in near–real time. NFLUX has three primary components: data processing, quality control, and 2D variational analysis. A schematic of the major components of the NFLUX radiative heat flux data flow is presented in Fig. 1. The steps after the first shaded rectangle are the same as for the turbulent heat fluxes presented in May et al. (2016), which discusses the quality control, 2D assimilation, and validation of the state parameters and turbulent heat fluxes.

a. Data processing

The first component of the NFLUX system for the radiative heat fluxes processes satellite swath-level data into swath-level surface downwelling shortwave and longwave estimates SW_{dwn} and LW_{dwn}, respectively. For full details on the production and evaluation of the NFLUX swath-level radiative heat flux estimates, refer to the companion paper (May et al. 2017). A brief summary is included here for completeness. The SW_{dwn} and LW_{dwn} swath-level estimates are produced using the Rapid Radiative Transfer Model for Global Circulation Models (RRTMG; Clough et al. 2005; Iacono et al. 2008). The primary inputs to the RRTMG are the swath-level atmospheric temperature and moisture profiles and cloud information obtained from the Microwave Integrated Retrieval System (MIRS; Boukabara et al. 2011). MIRS is available for six satellite platforms: the Defense Meteorological Satellite Program (DMSP) *F16* and *F18* platforms, the European Organisation for the Exploitation of Meteorological Satellites (EUMETSAT) *MetOp-A* and *MetOp-B* platforms, and the National Oceanic and Atmospheric Administration (NOAA) *NOAA-18* and *NOAA-19* platforms. Additional model inputs to the RRTMG include aerosol optical depths from the NRL Aerosol Analysis and Prediction System (NAAPS; Zhang et al. 2008), atmospheric ozone profiles from the Stratosphere Monitoring Ozone Blended Analysis (SMOBA; Yang et al. 2006), and sea surface temperatures (SST) from the U.S. Navy Global Ocean Forecasting System (GOFS; Metzger et al. 2014). Other inputs include trace gas amounts reported by the World Meteorological Organization (Dlugokencky et al. 2014), ocean surface albedo, ocean surface emissivity, and the solar constant.

The SW_{dwn} swath-level estimates obtained from the RRTMG are converted into clearness-index (CI)
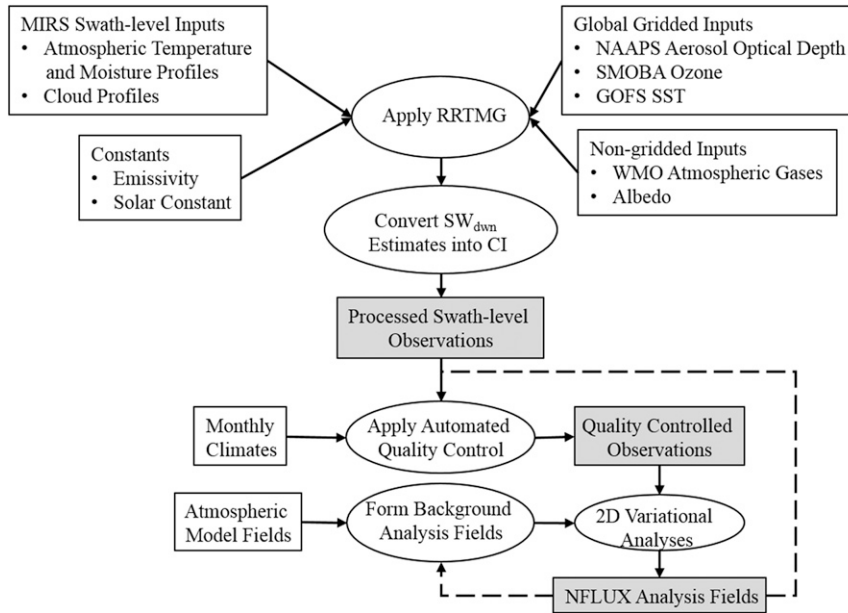
FIG. 1. The NFLUX system radiative heat flux data-flow schematic. Unshaded rectangles signify the input datasets, ovals signify major internal processes, and shaded rectangles signify the end product from each primary component of the NFLUX system. The dashed arrow lines indicate that the end product from one cycle is used in the following cycle.

values. The CI, also called the shortwave atmospheric transmittance, is defined as the ratio of the SW_{dwn} to the incoming solar radiation at the top of atmosphere SW_{TOA} and is representative of an atmospheric attenuation factor (Liou 1992; Petty 2006; Diagne et al. 2013; Inman et al. 2013; Boilley and Wald 2015). The advantage of CI over SW_{dwn} is that CI reduces the dependence on solar zenith angle, allowing CI values over a given time window to be considered as synoptic, which is not the case for SW_{dwn}.

b. Quality control

The second component of the NFLUX system applies an automated quality control (QC) to the swath-level CI and LW_{dwn} estimates. The NFLUX radiative heat flux QC process is an extension of the Navy Coastal Ocean Data Assimilation (NCODA) system (Cummings 2005; Cummings and Smedstad 2013) and follows the same method as described for the NFLUX turbulent heat fluxes (May et al. 2016). Prior to the QC, preliminary data sensibility checks are performed. These checks ensure that the data point is over the ocean, the observation location is consistent with prior positions from the same platform, the value is within valid ranges, and there are no duplicate reports. The QC process then assigns a probability of error ranging from 0 to 1, with 1 representing a high probability of error, to each valid observation on the basis of background-field checks.

The background-field checks include comparisons of the observations with the previous analysis, or forecast, field as well as with climatological values (described in more detail below). The final assignment of probability of error summarizes the results from all of the QC tests. If the observation fails the climate background check but not the previous-analysis field check, it is not necessarily assigned a low probability of error. As discussed in Cummings (2005), this QC process is designed to ensure that erroneous data will be assigned a high probability of error without excluding extreme but still valid data, which can be assigned a low probability of error if consistent with recent analysis or forecast fields.

For the radiative heat fluxes, the background-field check uses monthly climate fields constructed from the CERES SYN1deg product (Rutan et al. 2015). This CERES product provides climate-quality 3-hourly-average (at 0130, 0430, etc., UTC) surface and profile radiant fluxes and cloud properties using a one-dimensional radiative transfer model. Primary inputs to the CERES radiative transfer model include Moderate Resolution Imaging Spectroradiometer (MODIS) observations from the *Terra* and *Aqua* satellite platforms, 3-hourly observations from geostationary satellite platforms, and atmospheric reanalysis data from the Global Modeling and Assimilation Office Goddard Earth Observing System (GEOS) Model. The CERES 3-hourly monthly-mean SW_{dwn}, SW_{TOA}, and LW_{dwn}
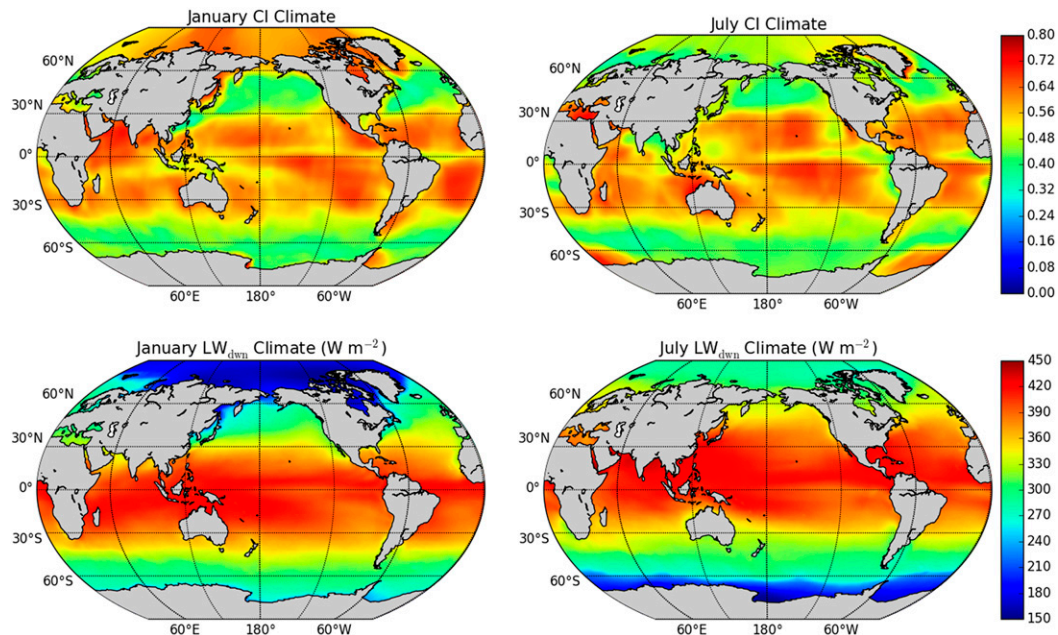
FIG. 2. (left) January and (right) July monthly climatological fields for (top) CI and (bottom) LW_{dwn}.

fields for July 2002–April 2015 were obtained from the NASA Langley Research Center Atmospheric Science Data Center. Three-hourly monthly-mean CI fields were created from the 3-hourly monthly-mean SW_{dwn} and SW_{TOA} fields (CI = SW_{dwn}/SW_{TOA}). Then, for each month of the year, a single monthly-mean CI (LW_{dwn}) field was created using a simple average of all CI (LW_{dwn}) 3-hourly monthly-mean values for the given month. This produced a total of 12 CI monthly-mean fields and 12 LW_{dwn} monthly-mean fields. A two-way five-point moving-average filter was then applied to the monthly-mean fields to reduce spatial noise. The January and July CI and LW_{dwn} monthly-mean climatological fields are shown in Fig. 2. These monthly-mean fields are used only in the QC checks.

c. 2D variational assimilation

The third component of the NFLUX system performs 2D variational analyses of the quality-controlled satellite swath-level CI and LW_{dwn} estimates with background fields from atmospheric model forecasts to produce global gridded analysis fields. Similar to the NFLUX QC component, the NFLUX 2D variational analysis component for the radiative fluxes is an extension of the NCODA system and follows the same method as described for the NFLUX turbulent heat fluxes (May et al. 2016, their section 2c). A discussion of the various aspects of the 2D variational analysis component is also provided here so that specific details related to the radiative heat fluxes, as opposed to the

turbulent heat fluxes, can be presented. The analysis fields are produced with a 3-hourly update cycle (i.e., 0000, 0300 UTC, etc.) from 10 April 2013 through 30 April 2014 on a Mercator projection with 24-km spacing along the equator. Although the grid only extends from 79.15°S to 79.15°N, we refer to the NFLUX product as being global since it covers the ice-free ocean.

As in May et al. (2016), the CI and LW_{dwn} 2D variational analyses are performed with a background field. The CI background field consists of only an atmospheric model forecast field of CI. The LW_{dwn} background field is formed by adding the weighted average of the previous 16 NFLUX LW_{dwn} analysis increment fields, representing 2 days, to an atmospheric model forecast field of LW_{dwn}. By including preceding increment fields in the background field, previously observed satellite-minus-model corrections are "persisted" forward. For consistency with May et al. (2016), the atmospheric model forecast fields used in this study are the NAVGEM 12-h forecast fields.

Parameter-specific background-field errors for CI and LW_{dwn} are modeled as a product of a background-error correlation length scale and a background-error variance, following May et al. (2016). The second-order autoregressive form is used as the analytical correlation structure in these results. The CI (LW_{dwn}) background-error correlation length scales were estimated using a time series of 3-hourly (12 hourly) NAVGEM forecasts and corresponding 12-h verifying analyses every 4 days (1 day) for 1 year (2013). At each verifying time, the
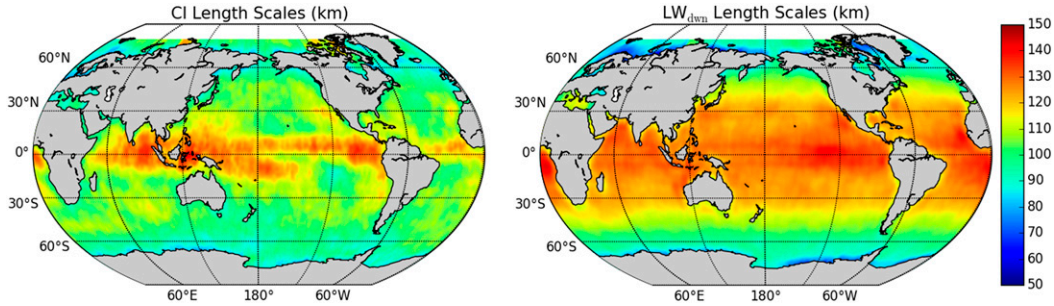
FIG. 3. NFLUX (left) CI and (right) LW_{dwn} horizontal length scales (km).

difference between the forecast field and verifying analysis field was defined as the error field. For each point on a uniform 2° grid, neighboring values from the error field were sorted into 50-km spatial-difference bins, from 50 to 500 km. A Gaussian function was fit to the binned covariances, with the characteristic scale of the Gaussian function taken to be the correlation length scale at that grid point. The time series of the fields of correlation length scale were then averaged together, and a two-way five-point moving-average filter was applied to create the final background-error correlation length scale fields (Fig. 3). The CI (LW_{dwn}) background-error variance at each analysis time is computed as the weighted sum of the previous 10 days of successive 24-hourly (3 hourly) forecast-field differences.

Before being assimilated with a background field, the satellite swath-level CI and LW_{dwn} observations must go through the automated QC. As discussed in section 2b, this process ultimately assigns a probability of error ranging from 0 to 1. All satellite swath-level CI and LW_{dwn} observations with a QC value of 0.95 or less and an observation time within 1.5 h of the NFLUX analysis time are assimilated with the background field, following the method of May et al. (2016). The QC threshold of 0.95 excludes only the observations with a very large probability of error; approximately 3% of the swath-level LW_{dwn} and 1% of the swath-level CI observations are excluded from assimilation.

For each analysis time, there are approximately 140 000 swath-level LW_{dwn} and 70 000 swath-level CI quality-controlled observations available for assimilation. Because of the amount of data available for assimilation, "super observations" are created for computational efficiency by averaging the input swath-level observations within bins that are 3 times the global analysis grid-mesh interval. In addition to the swath-level QC values, platform-specific observation errors are used to determine the weight of each observation. The observation errors are defined as the root-mean-square error (RMSE) of the swath-level retrievals when compared with in situ data. These errors are presented and discussed in detail in the companion paper (May et al. 2017). For completeness, the RMSEs from the combined in situ comparisons for each platform are shown in Table 1. For locations and times for which no satellite data are assimilated, the background field is not updated and effectively persists forward.

As discussed previously, an SW_{dwn} field, and not a CI field, is used to force ocean forecast models. After the CI analysis field is created, it is converted into an SW_{dwn} analysis field using $SW_{dwn} = CI \times SW_{TOA}$. The CI analysis fields are only considered to be an intermediate stage in the NFLUX system; the SW_{dwn} analysis fields are the product evaluated in this study.

3. NAVGEM

The U.S. Navy's current global atmospheric forecast and data assimilation system is NAVGEM (Hogan et al. 2014). For full details on the NAVGEM system used within NFLUX, the reader is referred to section 3 of May et al. (2016). The retrieved NAVGEM fields used in this study include the net surface shortwave radiation SW_{net}, net surface longwave radiation LW_{net}, and SST forecast fields. The NAVGEM CI field (again, CI = SW_{dwn}/SW_{TOA}), which is used as the NFLUX CI background field, is determined from the NAVGEM-calculated SW_{dwn} and SW_{TOA} fields:

$$SW_{dwn} = \frac{SW_{net}}{1 - 0.09} \quad \text{and} \tag{1}$$

$$SW_{TOA} = S_0 (r_0/r)^2 \cos Z, \tag{2}$$

where S_0 is the solar constant, r_0 is the mean sun–Earth distance, r is the instantaneous sun–Earth distance, which varies throughout the year according to the elliptical orbit, and Z is the solar zenith angle. The NAVGEM SW_{dwn} is calculated from SW_{net} using a constant ocean surface albedo of 0.09. We use a constant albedo to determine the NAVGEM SW_{dwn} since the

TABLE 1. Satellite swath-level observation errors by platform.

Platform	CI RMSE	LW_{dwn} RMSE (W m^{-2})
DMSP *F16*	0.17	22.11
DMSP *F18*	0.14	21.66
MetOp-A	0.13	18.93
MetOp-B	0.14	19.59
NOAA-18	0.15	20.33
NOAA-19	0.14	20.31

albedo over the ocean is set to a fixed value within the NAVGEM system (J. Ridout 2013, personal communication). The swath-level CI values that will be assimilated have been calculated using a varying ocean surface albedo (May et al. 2017).

The NAVGEM LW_{dwn} field,

$$LW_{dwn} = (\sigma T_s^4) - \frac{LW_{net}}{0.997}, \qquad (3)$$

where σ is the Stefan–Boltzmann constant (5.669×10^{-8} W m^{-2} K^{-4}) and T_s is the SST, is used as part of the NFLUX LW_{dwn} background field and is determined from the NAVGEM-provided LW_{net} and SST forecast fields and a constant ocean surface emissivity of 0.997. Similar to the NAVGEM ocean surface albedo discussed above, the ocean surface emissivity is also set to a constant value within the NAVGEM system (J. Ridout 2013, personal communication). The swath-level LW_{dwn} values that will be assimilated have also been calculated using a constant ocean surface emissivity value of 0.997. Using a varying ocean surface emissivity, which would be more realistic, will be investigated in future work.

4. Comparisons with in situ observations

In situ radiative flux observations are obtained from research vessels and moored buoys. The research-vessel observations in this study are from ships that participate in the Shipboard Automated Meteorological and Oceanographic System (SAMOS) initiative (Briggs et al. 2016). The moored-buoy observations are from four different arrays: the OceanSites network (http://www.oceansites.org), the Prediction and Research Moored Array in the Tropical Atlantic array (PIRATA; Bourlès et al. 2008), the Research Moored Array for African–Asian–Australian Monsoon Analysis and Prediction (RAMA; McPhaden et al. 2009), and the Tropical Atmosphere Ocean/Triangle Trans-Ocean Buoy Network array (TAO/TRITON; McPhaden et al. 1998). For the time period in this study, 12 research vessels and 47 moored buoys provided high-temporal-resolution SW_{dwn} observations while 9 research vessels and 14 moored buoys provided high-temporal-resolution

LW_{dwn} observations. Gupta et al. (2004) recommended averaging cloudy SW_{dwn} observations over 60 min to better represent the cloud spatial variability. In this study, there is no distinction between clear and cloudy conditions, and therefore all SW_{dwn} in situ observations have been averaged over 60 min. The LW_{dwn} in situ observations have no averaging applied. Further details on the locations of the in situ data and how the data were obtained can be found in section 4 of May et al. (2017).

The NFLUX (NAVGEM) global gridded SW_{dwn} and LW_{dwn} fields are validated against the in situ observations for 1 year, from 1 May 2013 through 30 April 2014. None of the in situ data have been assimilated into NFLUX or NAVGEM. The NFLUX CI global gridded fields are not evaluated since they are considered to be an intermediate product. The calculated error statistics include the NFLUX and NAVGEM mean, mean bias, standard deviation of the difference, RMSE, mean absolute percent error (MAPE), and correlation coefficient. The error-statistic equations are presented and discussed in May et al. (2016) and in the companion paper to this one (May et al. 2017). A positive bias indicates an overestimation by NFLUX or NAVGEM, and a negative bias indicates an underestimation by NFLUX or NAVGEM.

a. 3-hourly comparisons

Only the in situ observations with the center of the averaging window matching the 3-hourly model analysis time are used for validation. This allows for the same in situ platform to be used multiple times per day (up to eight times). The NFLUX and NAVGEM model fields are horizontally interpolated to the in situ observation location. The error statistics are presented for each in situ data type, as well as for the combination of all in situ data types. Since the in situ data types sample different latitude regions, the error statistics by in situ data type provide information on the range of conditions sampled.

1) DOWNWELLING SURFACE SHORTWAVE RADIATION

A total of 34 495 in situ observations are used to validate the 3-hourly SW_{dwn} fields. Error statistics between the NFLUX and NAVGEM 3-hourly global gridded SW_{dwn} fields and the in situ observations are presented in Table 2, with corresponding graphical comparisons shown in Fig. 4.

In the mid- to high latitudes, NFLUX has a lower absolute mean bias than NAVGEM. The NFLUX (NAVGEM) versus SAMOS and OceanSites matchups have mean bias values of 9.29 (24.17) and −11.99 (14.88) W m^{-2}, respectively. In the tropics, NFLUX has a higher (lower)

TABLE 2. Comparisons of the NFLUX and NAVGEM gridded 3-hourly SW_{dwn} estimates with in situ surface observations. Error statistics ($W\,m^{-2}$) are shown for each in situ type, as well as a combined type that represents the combination of all five in situ types. The error statistics include number of observations N, mean, mean bias, standard deviation (SD), RMSE, MAPE, and correlation coefficient squared R^2.

In situ type	N	Mean	Bias	SD	RMSE	MAPE	R^2
			NFLUX				
SAMOS	9133	350.60	9.29	136.07	136.39	58.03	0.89
OceanSites	6408	385.50	−11.99	126.80	127.37	38.88	0.90
PIRATA	16 363	497.64	23.97	143.19	145.19	43.69	0.88
RAMA	1646	500.37	46.00	163.35	169.70	52.88	0.85
TAO/TRITON	945	497.90	−45.20	129.18	136.86	26.71	0.91
Combined	34 495	438.02	12.56	140.24	140.80	46.57	0.89
			NAVGEM				
SAMOS	9133	365.48	24.17	151.15	153.07	69.78	0.86
OceanSites	6408	412.37	14.88	145.47	146.23	50.30	0.88
PIRATA	16 363	466.34	−7.33	165.32	165.49	49.09	0.83
RAMA	1646	454.73	0.36	188.47	188.47	77.94	0.79
TAO/TRITON	945	432.17	−110.93	146.62	183.86	28.92	0.89
Combined	34 495	428.12	2.66	160.56	160.59	55.62	0.85

absolute mean bias than NAVGEM with respect to the PIRATA and RAMA (TAO/TRITON) moored-buoy observations. The NFLUX (NAVGEM) versus PIRATA, RAMA, and TAO/TRITON matchups have mean bias values of 23.97, 46.00, and −45.20 (−7.33, 0.36, and −110.93) $W\,m^{-2}$, respectively. The NFLUX swath-level flux estimates, which are assimilated with the NAVGEM background fields, underestimate the total cloud coverage in the tropics (May et al. 2017). This results in generally positively biased swath-level observations being assimilated, which in turn causes the NFLUX biases to have a positive offset relative to the biases from NAVGEM in the tropics.

The NFLUX combined RMSE is smaller than the NAVGEM combined RMSE by 12.32%. The NFLUX RMSE ranges from 127.37 to 169.70 $W\,m^{-2}$ depending on in situ data type, with a combined RMSE of 140.80 $W\,m^{-2}$ [32.15%, where the percentage differences (Rutan et al. 2015) given here and below are calculated as RMSE/mean]. The NAVGEM RMSE ranges from 146.23 to 188.47 $W\,m^{-2}$ depending on in situ data type, with a combined RMSE of 160.59 $W\,m^{-2}$ (37.51%). The dominant feature to determine the quality of SW_{dwn} at shorter time scales is the diurnal cycle of the cloud fraction (Zhang et al. 1995; Long and Ackerman 2000; Trenberth et al. 2009; Rutan et al. 2015). The large RMSE values here suggest that the models are unable to accurately represent the diurnal cycle of the cloud fraction. Although NFLUX has large RMSE values, and a significant amount of scatter can be seen in the top panel of Fig. 4, NFLUX does show improvement over NAVGEM. Also, the percentage differences compare well with previous studies using the CERES SYN1deg products (Rutan et al. 2015).

As with the RMSE, NFLUX has smaller errors than NAVGEM for the remaining error statistics. The NFLUX (NAVGEM) R^2 ranges from 0.85 to 0.91 (0.79–0.89) for the various in situ data types, with a combined R^2 of 0.89 (0.85). NFLUX and NAVGEM in comparison with the TAO/TRITON moored buoys have the lowest MAPE values (least amount of error), and NFLUX and NAVGEM in comparison with the SAMOS research vessels and the RAMA moored buoys have the largest MAPE values (highest amount of error). This result indicates that the models compare better to the TAO/TRITON moored buoys in the tropical Pacific Ocean than to the other in situ data types.

As seen in the top and middle panels of Fig. 4, both NFLUX and NAVGEM show a general linear relationship with the in situ observations. The NFLUX comparisons have less scatter and a higher degree of correlation than the NAVGEM comparisons throughout the sampled range. This is consistent with NFLUX having improved error statistics relative to NAVGEM. To further investigate the NFLUX and NAVGEM SW_{dwn} comparisons, the in situ observations were sorted and divided into 15 equally populated bins. The bias and RMSE were then calculated for each bin and are shown in the bottom panel of Fig. 4. The general trends of NFLUX and NAVGEM are very similar. The NFLUX RMSE is smaller than the NAVGEM RMSE throughout the sampled range. Relative to NAVGEM, NFLUX has a smaller positive bias at locations with SW_{dwn} below approximately 300 $W\,m^{-2}$, a larger positive bias at locations with SW_{dwn} between 300 and 600 $W\,m^{-2}$, and a smaller negative bias at locations with SW_{dwn} above approximately 600 $W\,m^{-2}$. As the mean in situ SW_{dwn} value increases, the closer the mean in situ sun is to being
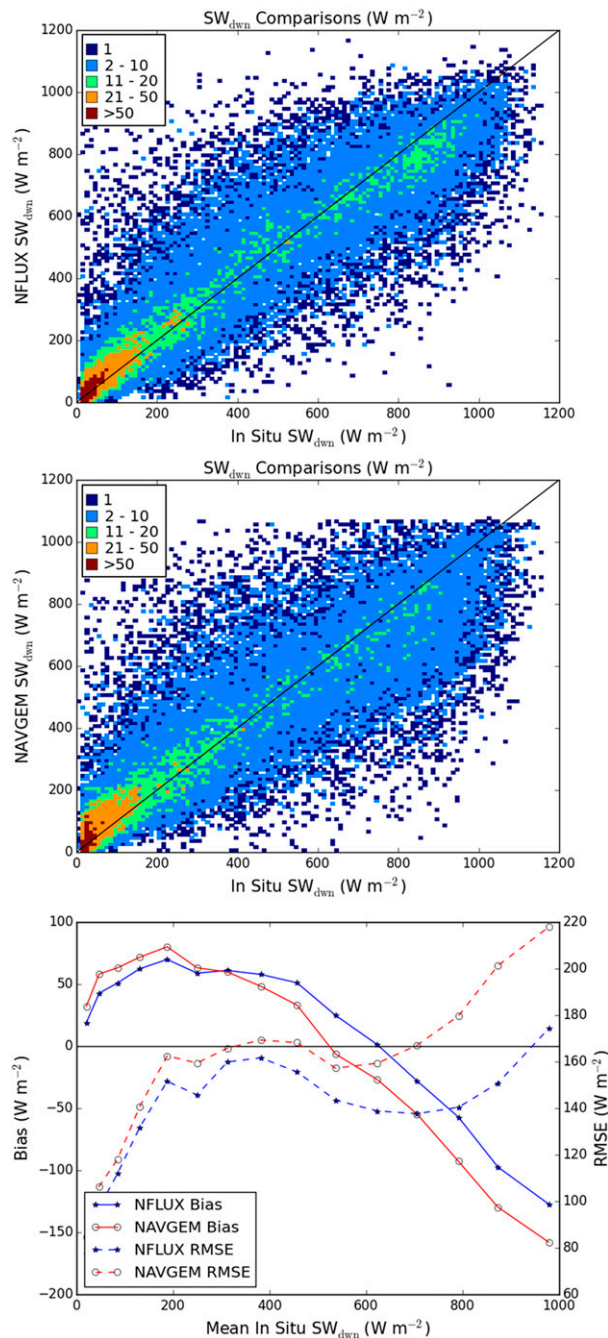
FIG. 4. Two-dimensional histograms for graphical comparison of (top) NFLUX and (middle) NAVGEM gridded SW_{dwn} estimates vs the combined in situ SW_{dwn} observations. The colors show the number of observations within each $10\,W\,m^{-2}$ bin. (bottom) The NFLUX and NAVGEM mean bias and RMSE statistics compared with the in situ observations that were sorted and divided into 15 equally populated bins.

directly overhead. As discussed before, cloud coverage has the largest impact on SW_{dwn}. The results here suggest that the atmospheric inputs to NFLUX misrepresent the diurnal cloud fraction, with a lack of clouds at locations

with SW_{dwn} below $600\,W\,m^{-2}$ (higher solar zenith angles) and an overabundance of clouds at locations with SW_{dwn} above $600\,W\,m^{-2}$ (lower solar zenith angles).

2) DOWNWELLING SURFACE LONGWAVE RADIATION

A total of 42 130 in situ observations are used to validate the 3-hourly LW_{dwn} fields. Error statistics between the NFLUX and NAVGEM 3-hourly global gridded LW_{dwn} fields and the in situ observations are presented in Table 3, with corresponding graphical comparisons shown in Fig. 5.

NFLUX has a smaller or similar absolute mean bias relative to NAVGEM for each in situ data type, which leads to NFLUX having a smaller combined mean bias ($-2.94\,W\,m^{-2}$) than NAVGEM ($-3.77\,W\,m^{-2}$). The atmospheric temperature and humidity are the primary sources of uncertainty in LW_{dwn}, with cloud coverage having less of an impact except at high latitudes (Zhang et al. 1995, 2006; Stephens et al. 2012). An increase in the low-level atmospheric temperature or water vapor increases the emission of longwave radiation from the atmosphere to the surface. The positive bias in NFLUX with respect to the TAO/TRITON moored buoys indicates that the low-level atmospheric inputs to NFLUX are too warm or too moist in the tropical Pacific. The negative bias in NFLUX relative to in situ observations outside the tropical Pacific indicates that the low-level atmospheric inputs to NFLUX are too cool or too dry.

NFLUX has smaller errors than NAVGEM does for all remaining calculated error statistics. The NFLUX combined RMSE is 16.64% smaller than the NAVGEM combined RMSE. The NFLUX RMSE ranges from 18.08 to $28.61\,W\,m^{-2}$ depending on in situ data type, with a combined RMSE from all in situ observations of $23.00\,W\,m^{-2}$ (6.14%). The NAVGEM RMSE ranges from 20.26 to $33.66\,W\,m^{-2}$ depending on in situ data type, with a combined RMSE from all in situ observations of $27.59\,W\,m^{-2}$ (7.34%). Similar to the SW_{dwn} percent differences, the LW_{dwn} percent differences also agree well with previous studies validating the CERES SYN1deg products (Rutan et al. 2015). The NFLUX (NAVGEM) R^2 ranges from 0.40 to 0.87 (0.26–0.85) for the various in situ data types, with a combined R^2 of 0.86 (0.85). NFLUX and NAVGEM in comparison with the PIRATA moored buoys have the lowest MAPE values, and the comparisons with the SAMOS research vessels have the highest MAPE values. This result indicates that the models compare better to the PIRATA moored buoys in the tropical Atlantic Ocean than to the other in situ data types.

Similar to the findings with the SW_{dwn} graphical comparisons, the NFLUX LW_{dwn} (top panel of Fig. 5) is

TABLE 3. As in Table 2, but for LW_{dwn}.

In situ type	N	Mean	Bias	SD	RMSE	MAPE	R^2
			NFLUX				
SAMOS	13 520	347.89	−5.05	28.16	28.61	6.19	0.87
OceanSites	13 052	370.68	−2.01	21.03	21.12	4.45	0.84
PIRATA	13 687	401.84	−3.24	17.79	18.08	3.46	0.54
TAO/TRITON	1871	394.60	7.91	20.72	22.18	4.85	0.37
Combined	42 130	374.55	−2.94	22.81	23.00	4.70	0.87
			NAVGEM				
SAMOS	13 520	341.29	−11.64	31.59	33.66	7.26	0.85
OceanSites	13 052	366.70	−5.99	26.47	27.13	5.73	0.80
PIRATA	13 687	408.27	3.19	20.01	20.26	4.07	0.47
TAO/TRITON	1871	404.30	17.61	22.35	28.46	6.42	0.26
Combined	42 130	373.72	−3.77	27.33	27.59	5.71	0.85

seen to have less scatter and a higher degree of correlation throughout the sampled range than does NAVGEM (middle panel of Fig. 5). This agrees well with NFLUX having improved LW_{dwn} error statistics relative to NAVGEM. To further investigate the NFLUX and NAVGEM LW_{dwn} comparisons, the in situ observations were sorted and divided into 15 equally populated bins. The bias and RMSE were then calculated for each bin and are shown in the bottom panel of Fig. 5. The overall trends of NFLUX and NAVGEM are similar. Except for the first and last two bins, NFLUX has a lower RMSE throughout the sampled range than NAVGEM. With respect to NAVGEM, NFLUX starts with a larger positive bias, has a smaller positive bias or a neutral bias at locations with LW_{dwn} from approximately 300 to 375 W m^{-2}, and then a larger negative bias at locations with LW_{dwn} above 375 W m^{-2}. As discussed before, the low-level atmospheric temperature and humidity have the most significant impact on LW_{dwn}. These results suggest that the low-level atmospheric inputs to NFLUX are too warm or that there is an overabundance of water vapor in regions where NFLUX overestimates LW_{dwn} (LW_{dwn} is below 325 W m^{-2}). Conversely, the low-level atmospheric inputs to NFLUX are too cool or there is a lack of water vapor in regions where NFLUX underestimates LW_{dwn} (LW_{dwn} is above 400 W m^{-2}).

To ensure consistency in the LW_{dwn} results, the NFLUX and NAVGEM combined errors were separated by night and day in Table 4. The NFLUX and NAVGEM mean values are very similar between night and day; the mean bias is higher for the daytime than for the nighttime, however. This could be a result of NFLUX (and NAVGEM) misrepresenting the diurnal warming. As stated before, NAVGEM uses a constant SST field throughout the forecast, which does not account for diurnal warming. The NFLUX LW_{dwn} background field includes these constant NAVGEM SST fields. The remaining errors for both NFLUX and

NAVGEM between day and night are very similar. The NFLUX nighttime and daytime RMSEs are within 0.14 W m^{-2}, with the percent difference for both nighttime and daytime being 6.14%. The NAVGEM nighttime and daytime RMSEs are within 0.12 W m^{-2}, with the percent difference for both nighttime and daytime being 7.38%. These results indicate good agreement between the nighttime and daytime LW_{dwn} matchups.

b. Daily comparisons

As discussed previously, the CERES SYN1deg products provide climate-quality surface fluxes. These products are provided at approximately a 6-month latency and are available for the time period in this study. The CERES 3-hourly products are provided at 0130 UTC, 0430 UTC, and so on, and the NFLUX and NAVGEM products are provided at 0000 UTC, 0300 UTC, and so on. Because of the mismatch in time, the 3-hourly products cannot be compared reliably. Daily averages of these products, however, can be compared. NFLUX daily averages are computed from the 3-hourly analysis fields. NAVGEM daily averages are computed from the 3-hourly forecast fields. The CERES SYN1deg daily averages were obtained from the NASA Langley Research Center Atmospheric Science Data Center. In situ daily observations are calculated for each platform that provided observations at least 90% of the day. The NFLUX, NAVGEM, and CERES model fields are horizontally interpolated to the in situ daily average latitude/longitude.

1) DOWNWELLING SURFACE SHORTWAVE RADIATION

A total of 13 039 daily in situ observations are used to validate the daily SW_{dwn} fields. Error statistics between the NFLUX, NAVGEM, and CERES daily global gridded SW_{dwn} fields and all in situ observations combined are presented in Table 5. Similar to the 3-hourly

FIG. 5. As in Fig. 4, but for LW_{dwn}. The colors in the 2D histograms now show the number of observations within each $2.5\,W\,m^{-2}$ bin.

TABLE 4. Comparisons of the NFLUX and NAVGEM gridded LW_{dwn} estimates with in situ surface observations. Error statistics ($W\,m^{-2}$) are as in Table 2 and are separated into nighttime and daytime.

Time	N	Mean	Bias	SD	RMSE	MAPE	R^2
			NFLUX				
Night	20 564	375.50	−1.83	23.00	23.07	4.77	0.86
Day	21 566	373.64	−3.99	22.58	22.93	4.64	0.87
			NAVGEM				
Night	20 564	374.65	−2.69	27.52	27.65	5.83	0.85
Day	21 566	372.84	−4.81	27.11	27.53	5.60	0.85

statistics. CERES has an RMSE of $30.98\,W\,m^{-2}$ (13.96%) and an R^2 of 0.92.

CERES SYN1deg ingests 3-hourly data from geostationary platforms in addition to imager data from polar-orbiting platforms to produce climate-quality products after a 6-month delay. NFLUX only uses microwave satellite data from polar-orbiting platforms to produce real-time products. As discussed before, the diurnal cycle of the cloud fraction largely determines the quality of SW_{dwn}. The microwave observations are less sensitive to thin clouds than are visible and infrared measurements (O'Dell et al. 2008; Aires et al. 2011). Also, the microwave-retrieved cloud liquid water in the NFLUX swath-level estimates is affected by the given particle size, whereas visible and infrared measurements are less affected by particle size (Boukabara et al. 2011; May et al. 2017). With these substantial differences between the NFLUX and CERES systems with respect to the types of satellites used and their abilities at cloud detection, it is expected that CERES will show better performance than NFLUX. The improvement from NAVGEM to NFLUX is approximately one-third of the improvement from NAVGEM to CERES.

Graphical comparisons between NFLUX, NAVGEM, and CERES daily global gridded SW_{dwn} fields and the in situ observations are shown in Fig. 6. The highest concentration of observations is seen at locations with daily SW_{dwn} between 200 and $300\,W\,m^{-2}$. The CERES comparisons (Fig. 6, bottom-left panel) show a high degree of correlation with little scatter. The NFLUX comparisons (Fig. 6, top-left panel) have more scatter and a smaller degree of correlation than the CERES comparisons. The NAVGEM comparisons (Fig. 6, top-right panel) have the most scatter and the lowest degree of correlation, relative to both the CERES and NFLUX comparisons. The in situ observations were sorted and divided into 15 equally populated bins. The bias and RMSE were calculated for each bin and are shown in the bottom-right panel of Fig. 6. The general trends among the three models are similar. As expected,

comparisons, NFLUX has smaller errors than NAVGEM does for all error statistics except for the mean bias. NFLUX has an RMSE of $53.31\,W\,m^{-2}$ (23.32%) and an R^2 of 0.74. NAVGEM has an RMSE of $60.44\,W\,m^{-2}$ (27.75%) and an R^2 of 0.64. The CERES SYN1deg product has smaller errors than NFLUX for all error

TABLE 5. Comparisons of the NFLUX, NAVGEM, and CERES gridded daily SW_{dwn} estimates with in situ surface observations. The error statistics (W m^{-2}) are as in Table 2.

Model	N	Mean	Bias	SD	RMSE	MAPE	R^2
NFLUX	13 039	228.59	15.82	50.91	53.31	27.24	0.74
NAVGEM	13 039	217.82	5.06	60.23	60.44	30.24	0.64
CERES	13 039	221.92	9.15	29.59	30.98	15.19	0.92

CERES has the smallest absolute value for the mean bias and the smallest RMSE throughout the sampled range. NAVGEM has a smaller bias or a similar positive bias in comparison with NFLUX at locations with daily SW_{dwn} below approximately 250 W m^{-2}. At locations with daily SW_{dwn} above 250 W m^{-2}, NFLUX has a smaller negative bias than NAVGEM. Each of the models has a positive (negative) bias at locations with daily SW_{dwn} below (above) approximately 250 W m^{-2}, which indicates that the models are overestimating (underestimating) the daily SW_{dwn}. This trend of NFLUX having a positive bias at low values of SW_{dwn} and a negative bias at higher values of SW_{dwn} is similar to the 3-hourly results discussed previously. NFLUX and NAVGEM have similar RMSE values at locations with daily SW_{dwn} below approximately 150 W m^{-2}. At locations with daily SW_{dwn} above 150 W m^{-2}, NFLUX has a smaller RMSE than NAVGEM does.

2) DOWNWELLING SURFACE LONGWAVE RADIATION

A total of 5237 daily in situ observations are used to validate daily LW_{dwn} fields. Error statistics between the NFLUX, NAVGEM, and CERES daily global gridded LW_{dwn} fields and the combined in situ observations are presented in Table 6. As with the LW_{dwn} 3-hourly comparisons, NFLUX shows improvement over NAVGEM for all error statistics. NFLUX has an RMSE of 19.99 W m^{-2} (5.35%) and an R^2 of 0.90. NAVGEM has an RMSE of 24.70 W m^{-2} (6.62%) and an R^2 of 0.87. CERES has an RMSE of 19.41 W m^{-2} (5.21%) and an R^2 of 0.90. Unlike the situation for the SW_{dwn} daily comparisons, the errors between NFLUX and CERES are very similar, with NFLUX having a smaller bias. Also, the improvement from NAVGEM to NFLUX is much greater than the improvement from NFLUX to CERES. This shows that NFLUX compares well to CERES for LW_{dwn}.

Graphical comparisons between NFLUX, NAVGEM, and CERES daily global gridded LW_{dwn} fields and the in situ observations are shown in Fig. 7. Similar to the 3-hourly LW_{dwn} comparisons, the highest concentration of observations is at locations where the observed daily LW_{dwn} is above 350 W m^{-2}. The NFLUX, NAVGEM,

and CERES comparisons each show a linear relationship with the in situ observations. The amount of scatter seen in each of the panels in Fig. 7 follows the same trend as seen in the SW_{dwn} daily comparisons. The NAVGEM comparisons (Fig. 7, top-right panel) have the largest amount of scatter. The NFLUX comparisons (Fig. 7, top-left panel) have less scatter and a higher degree of correlation relative to the NAVGEM comparisons. The CERES comparisons (Fig. 7, bottom-left panel) have the least amount of scatter and highest degree of correlation, in comparison with the NAVGEM and NFLUX comparisons. The in situ observations were sorted and divided into 15 equally populated bins. The bias and RMSE were calculated for each bin and are shown in the bottom-right panel of Fig. 7. The general trends among the three models are similar. NFLUX has the smallest absolute bias at locations with daily LW_{dwn} ranging from approximately 300 to 400 W m^{-2}. NAVGEM has the smallest absolute mean bias at locations with daily LW_{dwn} below 300 W m^{-2} and above 400 W m^{-2}. The CERES absolute mean bias is consistently between the NFLUX and NAVGEM absolute mean bias throughout the sampled range. NFLUX shows a positive (negative) bias at locations with daily LW_{dwn} below (above) 325 W m^{-2}, indicating NFLUX underestimates (overestimates) daily LW_{dwn}. These results are similar to those from the 3-hourly matchups, with NFLUX having a positive bias at lower LW_{dwn} values and a negative bias at higher LW_{dwn} values. NFLUX and CERES have very similar RMSE values throughout the sampled range, with NAVGEM having the largest RMSE throughout the sampled range.

5. Summary and conclusions

The NFLUX system produces satellite-based surface heat flux products over the global ocean in near–real time. The production of the NFLUX satellite-based turbulent latent and sensible heat fluxes, as well as the state parameters, is presented and discussed in Van de Voorde et al. (2015) and May et al. (2016). The production of the NFLUX swath-level shortwave and longwave radiative heat fluxes is presented and discussed in May et al. (2017). This study presents and discusses the NFLUX satellite-based global gridded radiative heat fluxes. As discussed by May et al. (2016), these NFLUX fields are designed to be an alternative to the NWP model fields, namely those from NAVGEM, that are used to provide the forcing for operational ocean models. These fields would also provide a basis for using satellite observations of
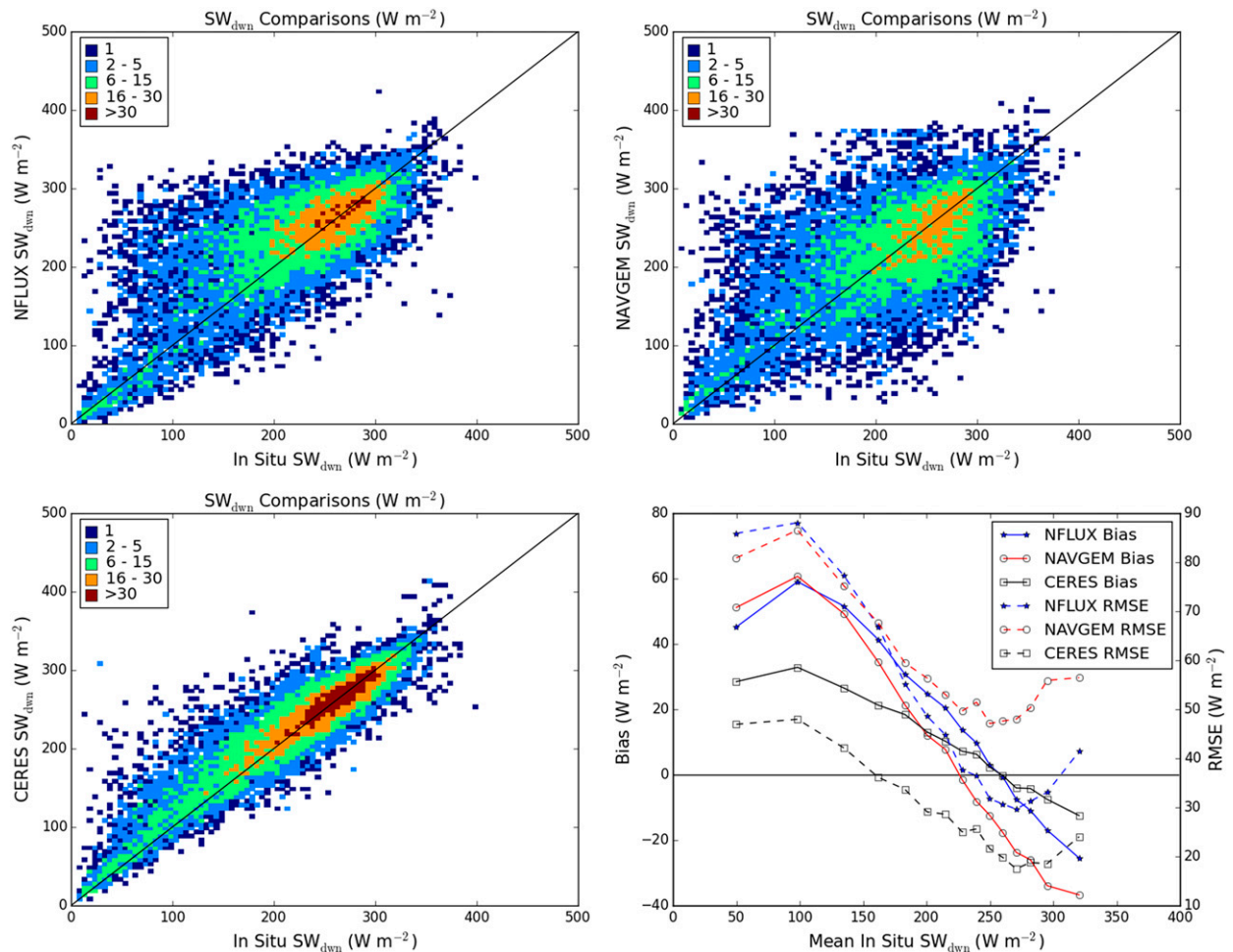
FIG. 6. Two-dimensional histograms for graphical comparison of (top left) NFLUX, (top right) NAVGEM, and (bottom left) CERES gridded daily SW_{dwn} estimates vs the combined in situ SW_{dwn} observations. The colors show the number of observations within each 5 W m^{-2} bin. (bottom right) NFLUX, NAVGEM, and CERES mean bias and RMSE statistics compared with the in situ observations that were sorted and divided into 15 equally populated bins.

the air–sea interface to assess and monitor NWP products.

The 3-hourly and daily NFLUX fields are evaluated for 1 year, May 2013–April 2014, relative to in situ observations from research vessels and moored buoys. NFLUX shows improvement over NAVGEM for each error statistic, except for some aspects of the absolute mean bias, for both the 3-hourly and daily comparisons. The 3-hourly SW_{dwn} (LW_{dwn}) NFLUX combined RMSE was 12.32% (16.64%) smaller than the NAVGEM combined RMSE. Examination of the NFLUX 3-hourly SW_{dwn} results revealed a positive (negative) bias at locations where the observed SW_{dwn} is below (above) 600 W m^{-2}, which is likely related to an underestimation (overestimation) in the diurnal cycle of the cloud fraction in the swath-level inputs to NFLUX. Examination of the NFLUX 3-hourly LW_{dwn} results

revealed a positive (negative) bias for locations at which the observed LW_{dwn} is below (above) 325 W m^{-2}, likely related to low-level atmospheric temperature inputs to NFLUX being too warm (cold) or low-level atmospheric moisture inputs to NFLUX being too high (low).

The daily NFLUX fields were also compared with the CERES SYN1deg daily average product. CERES provides climate-quality products in a 6-month delayed mode. Given the differences in the NFLUX and CERES

TABLE 6. As in Table 5, but for LW_{dwn}.

Model	N	Mean	Bias	SD	RMSE	MAPE	R^2
NFLUX	5237	373.92	−1.98	19.89	19.99	3.48	0.90
NAVGEM	5237	372.95	−2.95	24.53	24.70	4.78	0.87
CERES	5237	372.24	−3.67	19.06	19.41	3.15	0.91
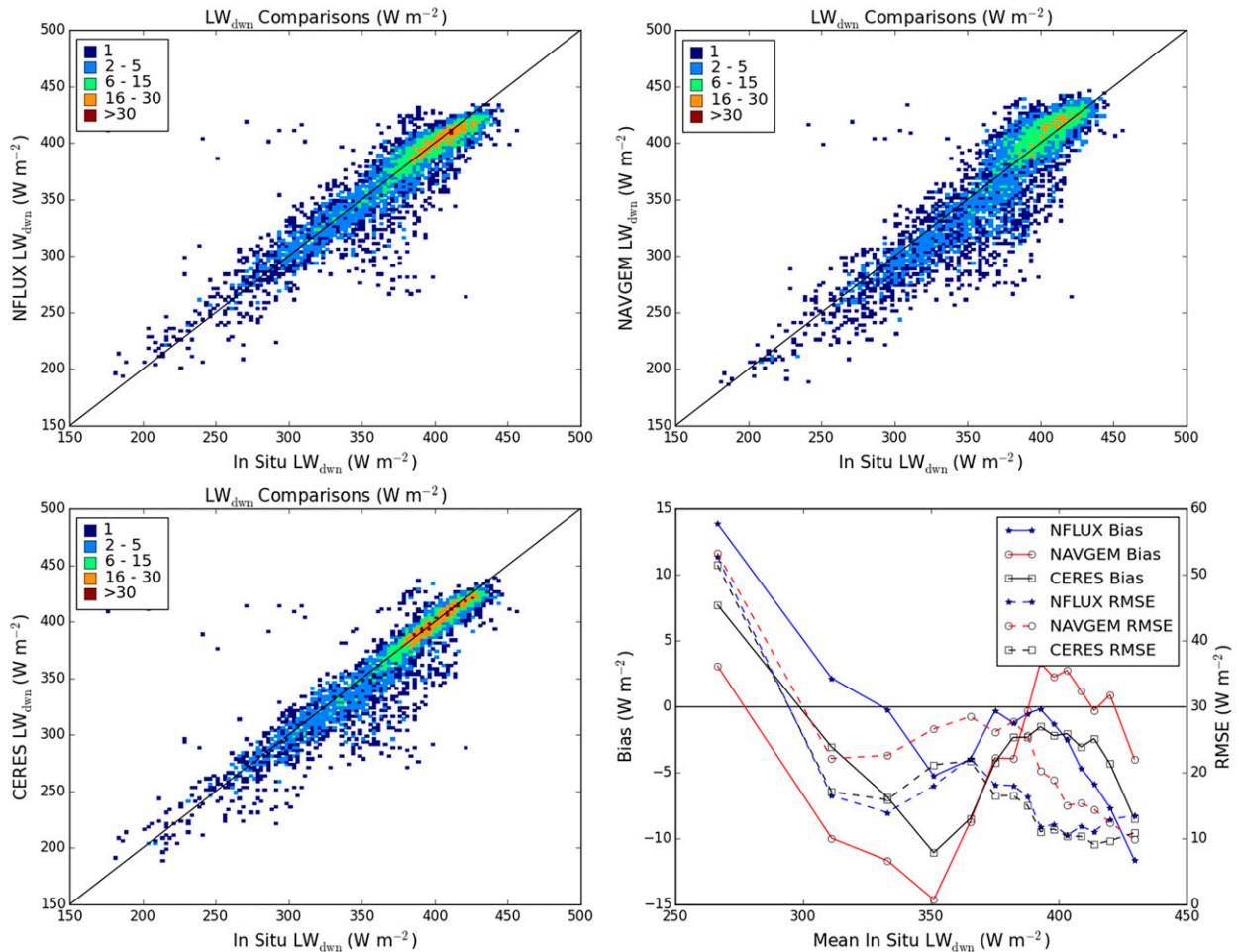
FIG. 7. As in Fig. 6, but for LW$_{dwn}$. The colors in the 2D histograms now show the number of observations within each 2.5 W m^{-2} bin.

products, the NFLUX fields compared reasonably well to CERES. The difference between NAVGEM and NFLUX is approximately one-third of the difference between NAVGEM and CERES for SW$_{dwn}$. For LW$_{dwn}$, the difference between NAVGEM and NFLUX is similar to the difference between NAVGEM and CERES.

This study completes the first version of the full suite of NFLUX satellite-based surface heat fluxes, from processing the raw satellite data through production of 3-hourly global gridded analysis fields. NFLUX has shown overall improvement relative to the current Navy global atmospheric model (NAVGEM) versus in situ datasets. Work is currently under way to determine the effect of using these NFLUX fields instead of the NAVGEM fields to provide surface forcing to ocean models. Future improvements in the production of the NFLUX radiative flux fields include using the new version-11 MIRS profile data, which have not yet been released for operational use, using a varying emissivity,

and incorporating the surface air temperature and moisture estimates from the NFLUX turbulent heat flux retrievals as part of the MIRS profile data.

REFERENCES

Aires, F., F. Marquisseau, C. Prigent, and G. Sèze, 2011: A land and ocean microwave cloud classification algorithm derived from AMSU-A and -B, trained using MSG-SEVIRI infrared and visible observations. *Mon. Wea. Rev.*, **139**, 2347–2366, doi:10.1175/MWR-D-10-05012.1.

Boilley, A., and L. Wald, 2015: Comparison between meteorological re-analyses from ERA-Interim and MERRA and measurements of daily solar irradiation at surface. *Renewable Energy*, **75**, 135–143, doi:10.1016/j.renene.2014.09.042.

Boukabara, S.-A., and Coauthors, 2011: MIRS: An all-weather 1DVAR satellite data assimilation and retrieval system. *IEEE*

Trans. Geosci. Remote Sens., **49**, 3249–3272, doi:10.1109/TGRS.2011.2158438.

Bourlès, B., and Coauthors, 2008: The PIRATA program: History, accomplishments, and future directions. *Bull. Amer. Meteor. Soc.*, **89**, 1111–1125, doi:10.1175/2008BAMS2462.1.

Briggs, K., S. R. Smith, and J. J. Rolph, 2016: 2015 SAMOS data quality report. Center for Ocean Atmospheric Prediction Studies Tech. Rep., 222 pp. [Available online at http://samos.coaps.fsu.edu/html/docs/2015SAMOSAnnualReport_final.pdf.]

Clough, S. A., M. W. Shephard, E. J. Mlawer, J. S. Delamere, M. J. Iacono, K. Cady-Pereira, S. Boukabara, and P. D. Brown, 2005: Atmospheric radiative transfer modeling: A summary of the AER codes. *J. Quant. Spectrosc. Radiat. Transfer*, **91**, 233–244, doi:10.1016/j.jqsrt.2004.05.058.

Cummings, J. A., 2005: Operational multivariate ocean data assimilation. *Quart. J. Roy. Meteor. Soc.*, **131**, 3583–3604, doi:10.1256/qj.05.105.

——, and O. M. Smedstad, 2013: Variational data assimilation for the global ocean. *Data Assimilation for Atmospheric, Oceanic and Hydrologic Applications*, S. K. Park and L. Xu, Eds., Vol. II, Springer-Verlag, 303–343, doi:10.1007/978-3-642-35088-7_13.

Curry, J. A., and Coauthors, 2004: SEAFLUX. *Bull. Amer. Meteor. Soc.*, **85**, 409–424, doi:10.1175/BAMS-85-3-409.

Diagne, M., M. David, P. Lauret, J. Boland, and N. Schmutz, 2013: Review of solar irradiance forecasting methods and a proposition for small-scale insular grids. *Renewable Sustainable Energy Rev.*, **27**, 65–76, doi:10.1016/j.rser.2013.06.042.

Dlugokencky, E. J., B. D. Hall, S. A. Montzka, G. Dutton, J. Muhle, and J. W. Elkins, 2014: Global climate: Long-lived greenhouse gases [in "State of the Climate in 2013"]. *Bull. Amer. Meteor. Soc.*, **95** (7), S33–S35. [Available online at http://journals.ametsoc.org/doi/pdf/10.1175/2014BAMSStateoftheClimate.1.]

Garratt, J. R., A. J. Prata, L. D. Rotstayn, B. J. McAvaney, and S. Cusack, 1998: The surface radiation budget over oceans and continents. *J. Climate*, **11**, 1951–1968, doi:10.1175/1520-0442-11.8.1951.

Gupta, S. K., D. P. Kratz, A. C. Wilber, and L. C. Nguyen, 2004: Validation of parameterized algorithms used to derive TRMM-CERES surface radiative fluxes. *J. Atmos. Oceanic Technol.*, **21**, 742–752, doi:10.1175/1520-0426(2004)021<0742:VOPAUT>2.0.CO;2.

Hogan, T. F., and Coauthors, 2014: The Navy Global Environmental Model. *Oceanography*, **27**, 116–125, doi:10.5670/oceanog.2014.73.

Iacono, M. J., J. S. Delamere, E. J. Mlawer, M. W. Shephard, S. A. Clough, and W. D. Collins, 2008: Radiative forcing by long-lived greenhouse gases: Calculations with the AER radiative transfer models. *J. Geophys. Res.*, **113**, D13103, doi:10.1029/2008JD009944.

Inman, R. H., H. T. C. Pedro, and C. F. M. Coimbra, 2013: Solar forecasting methods for renewable energy integration. *Prog. Energy Combust. Sci.*, **39**, 535–576, doi:10.1016/j.pecs.2013.06.002.

Kara, A., A. Wallcraft, and H. Hurlburt, 2007: A correction for land contamination of atmospheric variables near land–sea boundaries. *J. Phys. Oceanogr.*, **37**, 803–818, doi:10.1175/JPO2984.1.

Kratz, D. P., P. W. Stackhouse, S. K. Gupta, A. C. Wilber, P. Sawaengphokhai, and G. R. McGarragh, 2014: The Fast Longwave and Shortwave Flux (FLASHFlux) data product: Single scanner footprint fluxes. *J. Appl. Meteor. Climatol.*, **53**, 1059–1079, doi:10.1175/JAMC-D-13-061.1.

Liou, K. N., 1992: *Radiation and Cloud Processes in the Atmosphere*. Oxford University Press, 504 pp.

Long, C. N., and T. P. Ackerman, 2000: Identification of clear skies from broadband pyranometer measurements and calculation of downwelling shortwave cloud effects. *J. Geophys. Res.*, **105**, 15 609–15 626, doi:10.1029/2000JD900077.

May, J. C., C. Rowley, and N. Van de Voorde, 2016: The Naval Research Laboratory ocean surface flux (NFLUX) system: Satellite-based turbulent heat flux products. *J. Appl. Meteor. Climatol*, **55**, 1221–1237, doi:10.1175/JAMC-D-15-0187.1.

——, ——, and C. N. Barron, 2017: NFLUX satellite-based radiative heat fluxes. Part I: Swath-level products. *J. Appl. Meteor. Climatol.*, **56**, 1025–1041, doi:10.1175/JAMC-D-16-0282.1.

McPhaden, M. J., and Coauthors, 1998: The Tropical Ocean-Global Atmosphere observing system: A decade of progress. *J. Geophys. Res.*, **103**, 14 169–14 240, doi:10.1029/97JC02906.

——, and Coauthors, 2009: RAMA: The Research Moored Array for African–Asian–Australian Monsoon Analysis and Prediction. *Bull. Amer. Meteor. Soc.*, **90**, 459–480, doi:10.1175/2008BAMS2608.1.

Metzger, E. J., and Coauthors, 2014: US Navy operational global ocean and Arctic ice prediction systems. *Oceanography*, **27**, 32–43, doi:10.5670/oceanog.2014.66.

O'Dell, C. W., F. J. Wentz, and R. Bennartz, 2008: Cloud liquid water path from satellite-based passive microwave observations: A new climatology over the global oceans. *J. Climate*, **21**, 1721–1739, doi:10.1175/2007JCLI1958.1.

Petty, G. W., 2006: *A First Course in Atmospheric Radiation*. 2nd ed. Sundog Publishing, 458 pp.

Rossow, W. B., and R. A. Schiffer, 1999: Advances in understanding clouds from ISCCP. *Bull. Amer. Meteor. Soc.*, **80**, 2261–2287, doi:10.1175/1520-0477(1999)080<2261:AIUCFI>2.0.CO;2.

Rutan, D. A., S. Kato, D. R. Doelling, F. G. Rose, L. T. Nguyen, T. E. Caldwell, and N. G. Loeb, 2015: CERES synoptic product: Methodology and validation of surface radiant flux. *J. Atmos. Oceanic Technol.*, **32**, 1121–1143, doi:10.1175/JTECH-D-14-00165.1.

Smith, S. R., P. J. Hughes, and M. A. Bourassa, 2011: A comparison of nine monthly air–sea flux products. *Int. J. Climatol.*, **31**, 1002–1027, doi:10.1002/joc.2225.

Stephens, G. L., M. Wild, P. W. Stackhouse Jr., T. L'Ecuyer, S. Kato, and D. S. Henderson, 2012: The global character of the flux of downward longwave radiation. *J. Climate*, **25**, 2329–2340, doi:10.1175/JCLI-D-11-00262.1.

Trenberth, K. E., J. T. Fasullo, and J. Kiehl, 2009: Earth's global energy budget. *Bull. Amer. Meteor. Soc.*, **90**, 311–324, doi:10.1175/2008BAMS2634.1.

Van de Voorde, N., J. May, and C. Rowley, 2015: NFLUX PRE: Validation of new specific humidity, surface air temperature, and wind speed algorithms for ascending/descending directions and clear or cloudy conditions. NRL Rep. NRL/MR/7320-15-9611, 30 pp. [Available online at http://www7320.nrlssc.navy.mil/pubs/2015/may1-2015.pdf.]

Wallcraft, A. J., A. B. Kara, H. E. Hurlburt, E. P. Chassignet, and G. H. Halliwell, 2008: Value of bulk heat flux parameterizations for ocean SST prediction. *J. Mar. Syst.*, **74**, 241–258, doi:10.1016/j.jmarsys.2008.01.009.

Wang, D., L. Zeng, X. Li, and P. Shi, 2013: Validation of satellite-derived daily latent heat flux over the South China Sea, compared with observations and five products. *J. Atmos. Oceanic Technol.*, **30**, 1820–1832, doi:10.1175/JTECH-D-12-00153.1.

Yang, S.-K., S. Zhou, and A. J. Miller, 2006: SMOBA: A 3-dimensional daily ozone analysis using SBUV/2 and TOVS

measurements. NOAA/NWS/Climate Prediction Center. [Available online at http://www.cpc.ncep.noaa.gov/products/stratosphere/SMOBA/smoba_doc.shtml.]

Zhang, J., J. S. Reid, D. L. Westphal, N. L. Baker, and E. J. Hyer, 2008: A system for operational aerosol optical depth data assimilation over global oceans. *J. Geophys. Res.*, **113**, D10208, doi:10.1029/2007JD009065.

Zhang, T., P. W. Stackhouse Jr., S. K. Gupta, S. J. Cox, J. C. Mikovitz, and L. M. Hinkelman, 2013: The validation of the GEWEX SRB surface shortwave flux data products using BSRN measurements: A systematic quality control, production and application approach. *J. Quant. Spectrosc. Radiat. Transfer*, **122**, 127–140, doi:10.1016/j.jqsrt.2012.10.004.

——, ——, ——, ——, and ——, 2015: The validation of the GEWEX SRB surface longwave flux data products using BSRN measurements. *J. Quant. Spectrosc. Radiat. Transfer*, **150**, 134–147, doi:10.1016/j.jqsrt.2014.07.013.

Zhang, Y.-C., W. B. Rossow, and A. A. Lacis, 1995: Calculation of surface and top of atmosphere radiative fluxes from physical quantities based on ISCCP data sets: 1. Method and sensitivity to input data uncertainties. *J. Geophys. Res.*, **100**, 1149–1165, doi:10.1029/94JD02747.

——, ——, ——, V. Oinas, and M. I. Mishchenko, 2004: Calculation of radiative fluxes from the surface to top of atmosphere based on ISCCP and other global data sets: Refinements of the radiative transfer model and the input data. *J. Geophys. Res.*, **109**, D19105, doi:10.1029/2003JD004457.

——, ——, and P. W. Stackhouse, 2006: Comparison of different global information sources used in surface radiative flux calculation: Radiative properties of the near-surface atmosphere. *J. Geophys. Res.*, **111**, D13106, doi:10.1029/2005JD006873.